Magnetic-Field-Assisted Projection Stereolithography for Three-Dimensional Printing of Smart Structures

Lu Lu
Mem. ASME
Department of Mechanical and Industrial Engineering,
University of Illinois at Chicago,
842 W Taylor Street, ERF 1076,
Chicago, IL 60607
e-mail: llu27@uic.edu

Ping Guo
Mem. ASME
Department of Mechanical and Automation Engineering,
The Chinese University of Hong Kong,
Hong Kong, China

Yayue Pan[1]
Mem. ASME
Department of Mechanical and Industrial Engineering,
University of Illinois at Chicago,
842 W Taylor Street, ERF 3025,
Chicago, IL 60607
e-mail: yayuepan@uic.edu

In this paper, an additive manufacturing (AM) process, magnetic field-assisted projection stereolithography (M-PSL), is developed for 3D printing of three-dimensional (3D) smart polymer composites. The 3D-printed magnetic field-responsive smart polymer composite creates a wide range of motions, opening up possibilities for various new applications, like sensing and actuation in soft robotics, biomedical devices, and autonomous systems. In the proposed M-PSL process, a certain amount of nano- or microsized ferromagnetic particles is deposited in liquid polymer by using a programmable microdeposition nozzle. An external magnetic field is applied to direct the magnetic particles to the desired position and to form the desired orientation and patterns. After that, a digital mask image is used to cure particles in photopolymer with desired distribution patterns. The magnetic-field-assisted projection stereolithography (M-PSL) manufacturing process planning, testbed, and materials are discussed. Three test cases, an impeller, a two-wheel roller, and a flexible film, were performed to verify and validate the feasibility and effectiveness of the proposed process. They were successfully fabricated and remote controls of the printed samples were demonstrated, showing the capability of printed smart polymer composites on performing desired functions. [DOI: 10.1115/1.4035964]

1 Introduction

Materials with properties engineered to change in a controlled and desired fashion with specific external stimuli, like an external voltage, a magnetic field, a change in *p*H, a stress change, a temperature change, a moisture change, or a change in concentration of chemical species, are called smart materials and have received wide attentions recently [1]. This paper is focused on magnetic field-responsive smart polymer composites. A number of striking phenomena can be produced by embedding magnetic particles into polymer with designed patterns, including tunable elastic properties, giant deformational effects, high elasticity, anisotropic elastic and swelling properties, and quick response to magnetic fields [2]. In particular, composites that show anisotropic behavior in terms of mechanical and magnetic properties could be used to create a wide range of motions, and to control the shape change and movements. It opens up possibilities for various new technological applications in several biomedical and industrial fields, e.g., controlled drug delivery systems, diagnostic medicine, muscle-like soft linear actuators, biomimetic devices, separation techniques, high-density memory devices, spintronic, actuators for robots, elastomer bearings, and vibration absorbers to name a few [3–11].

However, manufacturing of such smart polymer composites that possess intelligence at the material level is still challenging. Material intelligence is referring to three main functions: sensing changes in environmental conditions, processing the sensed information, and finally actuating by moving away from or to the stimulus [1,2]. Conventional manufacturing technologies for smart polymer composite products include wet lay-up, resin transfer molding (RTM), autoclave processing, resin film infusion, filament winding, prepreg method, etc., [7]. Despite advancements and efforts in polymer composite manufacturing in last two decades, a number of issues such as 3D part production, heterogeneous composites fabrication, intensive labor, and so on, still exist [7,12].

Additive manufacturing (AM), which is also known as 3D printing or solid freeform fabrication, is a class of technologies that builds parts layer by layer using digital 3D design data. Comparing with the traditional manufacturing technologies, AM offers many unique advantages in terms of material/energy efficiency, mold-free operation style, design flexibility, and so on [13]. In last decade, many efforts have been made on developing AM technologies for polymer composites fabrication. For example, Khalil et al. [14] presented a multinozzle deposition system to 3D print polymer composite, and Zhou et al. [15] developed a multimaterial mask-image-projection-based stereolithography (SL) system that is capable of curing multiple liquid resins in a build job to produce multipolymer materials. Furthermore, Beaman and Das groups investigated selective laser sintering for polymer composite fabrication using multiple polymer powder materials [16–19].

As a multiscale and fast additive manufacturing method, stereolithography (SL) related processes have also been developed to process a mixture of metallic/polymer particles and liquid [20–22]. In the process of 3D printing particle–polymer composites using SL-related technologies, the printing job usually starts with mixing the filler particles with liquid photopolymers by various methods like ultrasonic mixing. Then, the mixture is polymerized by a laser beam or patterned light in a layer-by-layer fashion. Such SL methods open new routes for fabricating various 3D ceramic products or smart polymer composite parts with homogeneous properties. Compared with other AM technologies, SL methods provide multiple scale manufacturing capabilities from nanoscale to meso-scale [23,24], smooth surface [25,26], and fast build speed [27,28]. However, mixing of particles and liquid resin remains the primary challenge, as agglomeration or undesired particle dispersion patterns occur when the particles are not blended properly before the printing or when the 3D printing

[1]Corresponding author.

Manuscript received November 7, 2016; final manuscript received February 2, 2017; published online March 8, 2017. Assoc. Editor: Zhijian J. Pei.

process takes a long time. Furthermore, because a whole tank of particle-resin suspension is prepared and is used for printing layers, the particle concentrations, and filling patterns are hardly to control among layers in a single print. Compared with the in situ particle-resin blending, such premixing manufacturing method lacks flexibilities in producing composites with heterogeneous properties, greatly limiting applications in smart machines.

Therefore, in this paper, we developed a magnetic field-assisted projection stereolithography (M-PSL) process, characterized by a layer-by-layer in situ particle resin mixing, and hence heterogeneous composite properties. With the assistance of an external magnetic field, it is possible to control local dispersions of magnetic particles in liquid photopolymer, and hence to fabricate material intelligence by patterning particles and localizing particle concentrations in the polymer matrix. The manufacturing process has been planned, and a testbed was developed. Three test cases were fabricated and discussed. The experimental results verified the feasibility of the fabricating magnetic field responsive smart polymer composites using the proposed method.

2 M-PSL Process Planning

The proposed magnetic field-assisted projection stereolithography (M-PSL) system is illustrated in Fig. 1. Same as the other additive manufacturing processes, the proposed M-PSL process starts with 3D computer-aided design (CAD) model of the object. The CAD model is sliced into a series of cross-sectional layers. The sliced layers are then converted to digital mask images that are sent to the digital micromirror device (DMD). The DMD is a micro-electromechanical system device that enables one to simultaneously control $\sim 1 \times 10^6$ small mirrors that turn on or off a pixel at over 5 kHz. For each cross-sectional slice of the object, the DMD projects patterned light that selectively exposes and hardens the resin. A layer of resin is cured into the shape defined by the related mask image to form a layer of the object. If that layer requires magnetic particles, a programmable pumping system and a micronozzle are used to deposit magnetic particle solution into the liquid resin vat. During this process, the volume of deposited magnetic particle is precisely controlled by the programmable pumping system, and particle filling patterns and ratios are determined by the external magnetic field. Because particles are blended into liquid resin in situ, fast build speeds, local magnetic intelligence, and heterogeneous properties could be achieved easily.

A flowchart of the magnetic field-assisted projection stereolithography (M-PSL) process is shown in Fig. 2. A digital model, containing not only structural information but also function information, could first be used to generate particle deposition images and curing images. Particle deposition images contain all information that are required for filling particles in the polymer matrix

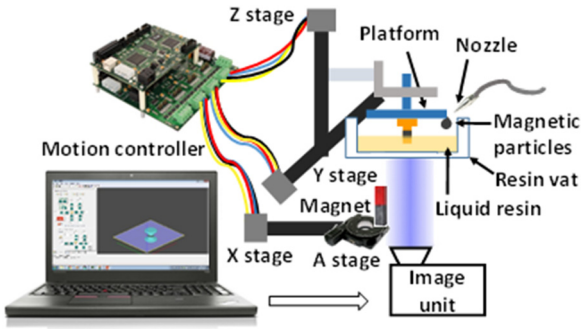

Fig. 1 A schematic diagram of the smart polymer composite printing system using M-PSL process: stage X to move the magnet along *X* axis and stage A to rotate the magnet around *Z* axis; stage Y and stage Z to move the platform along *Y* and *Z* axis

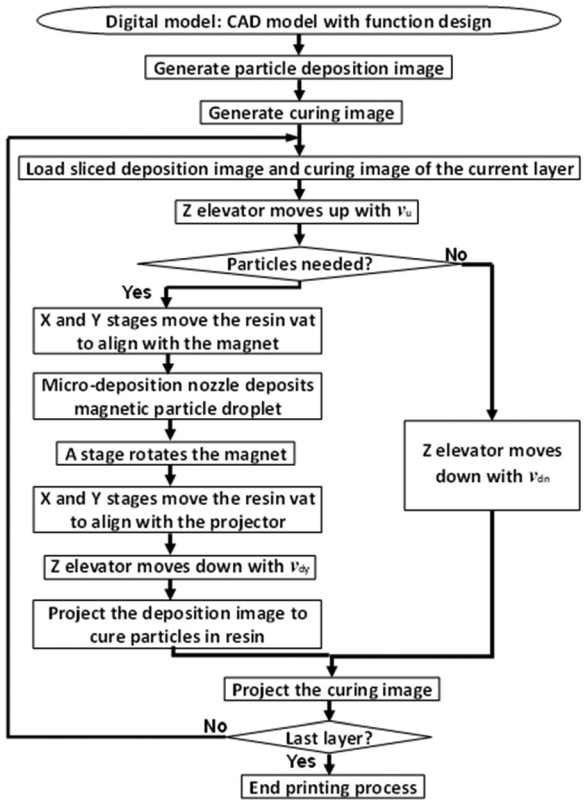

Fig. 2 Flowchart of the M-PSL process

properly to achieve the designed functions. In particular, such information includes filling areas and loading fractions of magnetic particles in each layer. Curing images determine curing parameters and patterns, like exposure time, cross section geometry, and layer thickness.

The generated particle deposition image and curing image of the current layer will be loaded into our main process control program, which was developed using the C++ language with Microsoft Visual Studio. *Z* elevator that carries the platform then moves up with a speed v_u. If the particle deposition image indicates that no particle is needed for that layer, *Z* elevator moves down with a relative fast velocity to form a layer of resin for curing. If the deposition image indicates that the current layer needs to be filled with particles, the resin vat will be aligned with magnet before depositing a desired amount of magnetic particles into the resin vat by a micronozzle. A dynamic magnetic field is then formed by rotating a magnet, attracting the magnetic particles to desired particle filling areas. Then, the resin vat moves back to projection area, and the *Z* elevator moves down to create a layer of resin with suspended particles. The moving down velocity v_{dy} is determined experimentally. To avoid disturbing the particle suspension, v_{dy} is much smaller than the moving-down speed v_{dn} for particle-free layers and moving-up speed v_u. After that, the deposition image will be transferred to the DMD-based imaging unit to cure particles in desired areas. After curing of particles, unwanted particles are removed by a moving magnetic field. Then, the curing image will be projected to cure the whole layer of liquid resin and particles with desired shapes. A 3D smart polymer composite product with digitally designed geometries and functions is then built by following this procedure and stacking 2D composite layers with controlled particle filling patterns and ratios.

3 Experimental Setup

3.1 Hardware System. As shown in Fig. 3(*a*), a M-PSL testbed was developed for printing magnetic field responsive

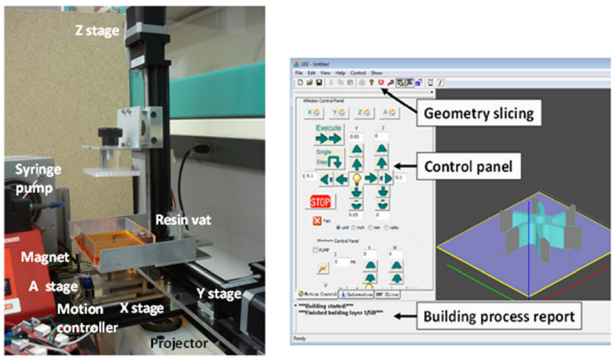

Fig. 3 A bottom-up projection SL setup: (*a*) hardware and (*b*) software

smart polymer composites. It consists of an imaging unit, a resin vat that has optic clear bottom surface, a linear actuator that elevates the build platform, two linear stages used for sliding the resin vat, a magnet that is mounted on a rotation stage, and a controller that is able to control four axis. To assist separation process, the bottom surface of liquid vat is coated with 2 mm thick polydimethylsiloxane (PDMS). An off-the-shelf projector was used as the imagining unit. The optical lenses of the projector were modified to reduce the projection distance. Various projection settings, including focus, key stone rectification, brightness, and contrast were adjusted to achieve a sharp projection image on the designed projection plane. The DMD resolution in our system is 1024×768, and the envelope size is 42.7×32 mm. A permanent magnet composed of grade 40 neodymium iron boron magnetic material is used in this testbed to direct the magnetic particles to desired locations.

3.2 Software System. A digital mask planning and process control testbed has been developed using the C++ language with Microsoft Visual Studio. The testbed integrates the geometry slicing, image generation, particle deposition controlling, and motion controlling. In this study, it is assumed that the CAD model with function design is given. The testbed also synchronizes the image projection with Z movements. The graphical user interface of the developed software system is shown in Fig. 3(*b*).

3.3 Materials. Two different magnetic particle solutions, a ferrofluid from CMS, Inc., and a magneto-rheological (MR) fluid MRF-122EG from Mid-Atlantic Rubber, Inc. (Baltimore, MD), were tested. It is found that the hydrocarbon-based magneto-rheological fluid MRF-122EG is easier to disperse with controlled patterns. Hence, it was selected as the magnetic particles used in test cases that are discussed in the experimental results section. MRF-122EG is a suspension of micron-sized, magnetizable iron particles in a carrier fluid. The iron particles content by weight is 72%. In MRF-122EG, the iron particles are between 1 and 20 μm. Response time for the MRF-122EG is less than 5 ms [29]. In the absence of a magnetic field, MRF-132EG fluid flows freely, exhibiting a viscosity of 0.042 Pa·s at 40 °C, and the particles suspend in the carrier fluid stably [29]. Upon application of a magnetic field, the rheology of MRF-122EG fluid reversibly and instantaneously changes from a free-flowing liquid to a semisolid with controllable yield strength. When exposed to a magnetic field, the fluid's particles align with the direction of the field in chain-like fashion, thereby restricting the fluid's movement within the gap in proportion to the strength of the magnetic field.

Three different photopolymers, 3DM-ABS from 3D Materials, Inc., E-shell 600 from EnvisionTEC, and FLGR01 from Formlabs, were tested in this study. Their properties are summarized in Table 1. With the same external magnetic field, particles move slower in the liquid resin with higher viscosity. When the resin viscosity is too high, it might be only portions of magnetic particles that move along the magnetic field lines. The response of magnetic particles in the three liquid resins was tested. The experimental results show that with a volume of 0.01 ml MR fluid and an external magnetic field of 10 kg, magnetic particles move by 10 mm in 5 s in 3DM-ABS, 10 s in E-shell 600, and 25 s in FLGR01.

Therefore, to validate the feasibility and test the capability of the proposed magnetic field-assisted projection stereolithography process, we performed test cases with the two resins with very different rheological and mechanical properties, 3DM-ABS and FLGR01, and the MR fluid MRF-122EG in the following experimental study.

4 Experimental Results and Discussion

Three test cases, an impeller, a two-wheel roller, and a switch, were performed. In all test cases, magnetic particles were designed to fill in the polymer matrix in certain areas, instead of being dispersed homogeneously in the whole part.

4.1 Test Case 1—Fabrication of an Impeller Using M-PSL

4.1.1 Model Design and Manufacturing Process. Figure 4(*a*) shows the digital design of the impeller model. The impeller is 24 mm in diameter and 5 mm in thickness. Magnetic particles are embedded at the tip of all the blades. The volume loading fraction of the magnetic particles is designed to be 0.002. The yellow area represents polymer material, and the gray area represents the particle–polymer composite material. Vector z represents the building orientation in our M-PSL process.

Layers with a thickness of 0.2 mm are sliced along the z direction. Figures 4(*b*) and 4(*c*) show the sliced deposition image and curing image. As discussed in Sec. 2, the manufacturing program will first check deposition image to see if particles are needed for that layer, and if yes, a certain volume of magnetic particle solution will be pumped through a micronozzle into the resin vat. In the deposition image, the gray scale value g is defined as a number between 0 and 1, indicating the volume loading fraction of particles in that pixel. The exact volume of magnetic particle solution that will be needed for that layer is calculated by the gray scale values g using the following equation:

$$V_{\text{particle}} = \sum_{i=I1}^{i=I2} \sum_{j=J1}^{j=J2} (g_{(i,j)} \times a_{(i,j)} \times d) \tag{1}$$

where V_{particle} is the volume of particles that will be filled into the area ($i \in (I1,\ I2),\ j \in (J1,\ J2)$), i is the pixel index in x direction, j is the pixel index in y direction, $g_{(i,j)}$ is the gray scale value (volume loading fraction) of pixel (i, j), $a_{(i,j)}$ is the area of the

Table 1 A summary of material properties

Properties	Effective light wave length (nm)	Viscosity at 25 °C	Mechanical properties	Color	Density at 25 °C (g/cm^3)
3DM-ABS	380–420	50 cP	Hard, tough	Translucent orange	1.12
E-shell 600	380–420	400 cP	Hard, tough	Clear	1.15
FLGR01	380–420	4500 cP	Flexible: Tensile strength 7.7–8.5 MPa	Light gray	1.09

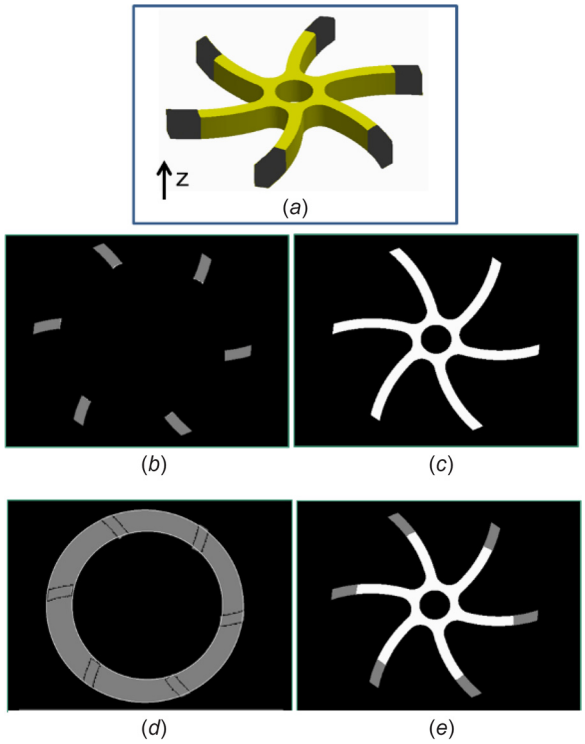

Fig. 4 Digital design and process planning for an impeller test case: (*a*) digital design, (*b*) sliced deposition image, (*c*) sliced curing image, (*d*) particle dispersion before curing, and (*e*) curing pattern

pixel (i, j), and d is the layer thickness. In our test cases, to ensure that the particle dispersion area will be fully covered, the actual deposition volume V_{dep} is calculated by multiplying V_{particle} with a coefficient k_{dep}

$$V_{\text{dep}} = V_{\text{particle}} \times k_{\text{dep}} \tag{2}$$

An empirical value 1.8 is used for the coefficient k_{dep} in all the test cases. In addition, if the particle filling pattern consists of multiple islands, the particle deposition will be performed separately for each island. For example, as shown in Fig. 4, in this test case, the tips of six blades require magnetic particles. The magnetic particle deposition volume V_{dep} is calculated separately for each blade. And particles are deposited and directed to the desired area to cover the tip fully. By following this procedure for each tip, particles will be dispersed in the six areas, as illustrated as the gray circles in Fig. 4(*d*).

After particle deposition, the deposition image will be projected to illuminate the particle filling regions, to cure particles in the resin. After the particle curing, the unwanted particles will be attracted by the external magnetic field and moved to a recycle corner of the tank. Then, the curing image will be projected to illuminate the whole cross section layer. In this test case, a 7 s was used as the exposure time for both deposition image and curing image. A 0.2 mm layer thickness was used.

4.1.2 Fabricated Results. The fabricated part is shown in Fig. 5(*b*). Microscopic images of the blade tip area and the central area are shown in Figs. 5(*c*) and 5(*d*). In the microscopic images, due to the filling of particles, the blade tip has a much darker color than the no-particle areas. The impeller body is fabricated as particle free. The experimental results show that a composite product with particles filled in the desired areas can be successfully fabricated using the proposed M-PSL process.

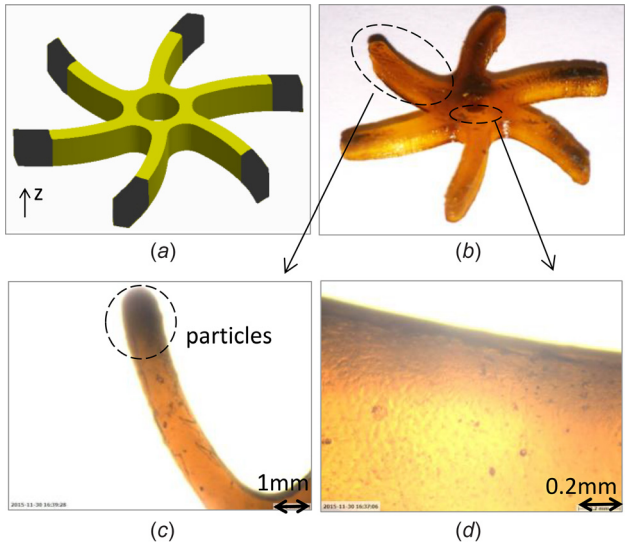

Fig. 5 Pictures of the fabricated impeller using the developed M-PSL process: (*a*) digital design, (*b*) printed part, (*c*) miroscopic image, and (*d*) microscopic image

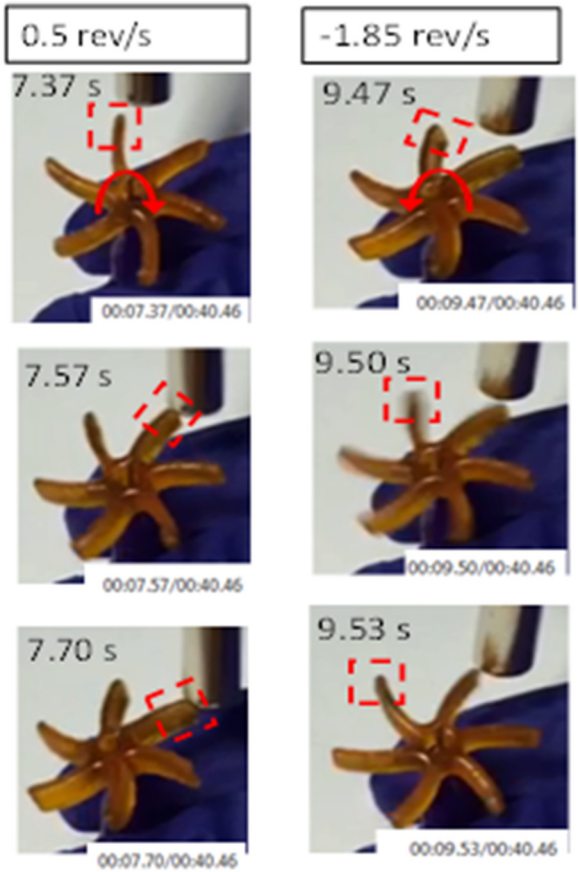

Fig. 6 Movements of the impeller under different external magnetic fields: (*a*) clockwise rotation and (*b*) counterclockwise rotation

4.1.3 Fabricated Material Intelligence and Functionality. A permanent magnet is used to trigger rotation movements of the fabricated impeller. The experimental results show that the clockwise and counterclockwise movements with various rotation speeds could be achieved. A 0.5 revolution per second clockwise

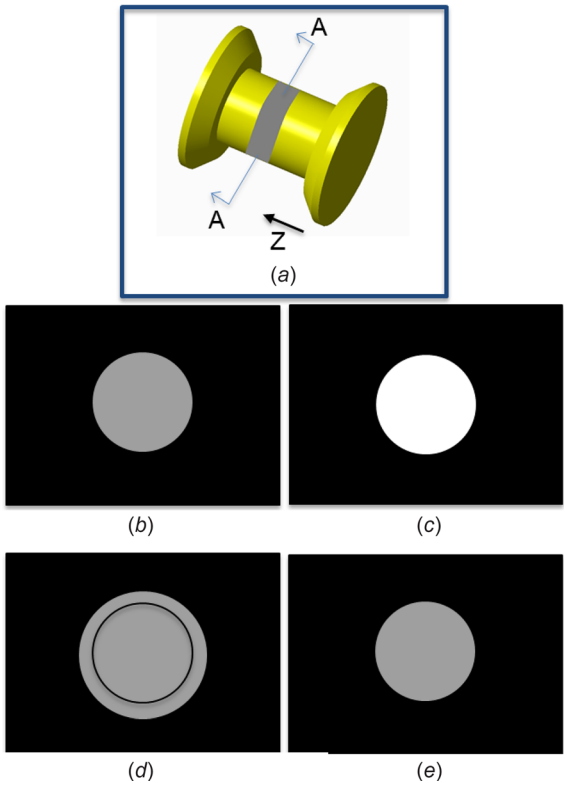

Fig. 7 Digital design and process planning for a two-wheel roller test case: (*a*) digital design, (*b*) sliced deposition image, (*c*) sliced curing image, (*d*) particle dispersion before curing, and (*e*) curing pattern

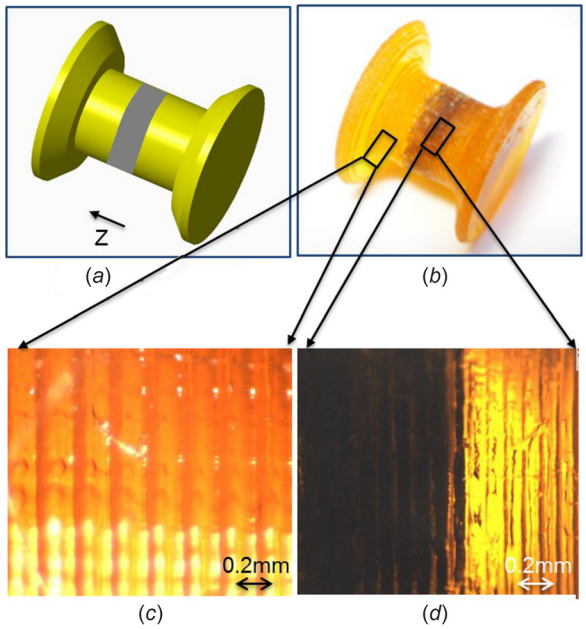

Fig. 8 Pictures of the fabricated rolling machine using the developed M-PSL process: (*a*) digital design, (*b*) printed part, (*c*) microscopic image of the particle-free layers, and (*d*) microscopic image of the particle-polymer composite layers

rotation example and a −1.85 revolution per second counterclockwise rotation example are shown in Fig. 6. For presentation effects, a red dashed block marks the same blade in all pictures to show rotation movements, and a red arrow is used to denote the rotation direction of each movement.

Experiments were performed to characterize the rotation accuracy of the impeller. Five replications were conducted. A camera was mounted in a way that top images of the rotating impeller could be taken. The rotation angle of the impeller was calculated by analyzing the captured top images and compared with the designed rotation angle. It was found that a rotation accuracy with an error of 0.05% ± 0.03% can be achieved on the printed impeller.

4.2 Test Case 2—Fabrication of a Two-Wheel Roller Using M-PSL

4.2.1 Model Design and Manufacturing Process. A two-wheel roller was also tested, to verify the capability of the proposed M-PSL process on fabricating smart polymer composite structure. As shown in Fig. 7(*a*), the roller is designed to have particles filled in the center of the connecting rod. The diameter for the wheel and rod are 14 mm and 7 mm, respectively. The part is 8.5 mm long. To differentiate the two wheels, different thicknesses are designed. Magnetic particles are only designed in the half of the rod that is connected with the thin wheel. By filling particles on the thin wheel end only instead of the whole part, a heterogeneous magnetic property could be created. As a result, the thin wheel will serve as a driving wheel.

The same manufacturing process and methods as described in the previous test case were adopted. For the cross section layer A–A which is filled with magnetic particles, the deposition image, curing image, particle dispersion area before curing, and curing pattern of particle–resin composite for layer A–A are shown in Figs. 7(*b*)–7(*e*). Exposure time was set as 7 s for all images. A layer thickness of 0.2 mm was used for slicing and building. Vector *z* in Fig. 7(*a*) denotes the building direction.

4.2.2 Fabricated Results. The two-wheel roller machine was fabricated successfully, as shown in Fig. 8. Microscopic images of the particle-free layers and the particle–polymer composite layers are shown in Figs. 8(*c*) and 8(*d*).

Different with the impeller test case where the particle deposition area for each layer is quite small (1.5 mm^2), this roller model requires a much bigger particle dispersion area for each layer (77 mm^2). Along with this relatively large dispersion area, the external magnetic field for directing particles needs to be controlled very carefully. If the external magnetic field is not uniform and consistent, a uniform distribution of particles cannot be achieved. Fabricated results of these test cases verified that the M-PSL process could fabricate both complicated structures and regular shape structures accurately, and the influence of magnetic particles on geometrical accuracy is negligible.

4.2.3 Fabricated Function and Remote Control of the Roller. A permanent magnet is used as an external stimulus to trigger the rolling movement of the impeller and remotely control it. By tuning the relative position of the magnet to the roller, the roller could move along various routes. In addition, the rolling speed could be adjusted in the range of 40–90 mm/s. Furthermore, due to the imbalance of magnetic force, the thin wheel is working as a driving wheel. Two rolling movement videos are shown in Fig. 9. The red-dashed arrow marks the rolling route in each group. It can be seen that the roller could be remotely controlled by the external magnetic field. Acceleration, rolling, different rolling speeds, and turning could be realized through remote control using external magnetic stimuli.

Experiments were conducted to characterize the rolling motion accuracy of the printed roller. The moving paths of the roller were recorded by a camera. By analyzing the captured moving path from the captured photos and comparing with the designed moving path, the maximum distance between the actual rolling path

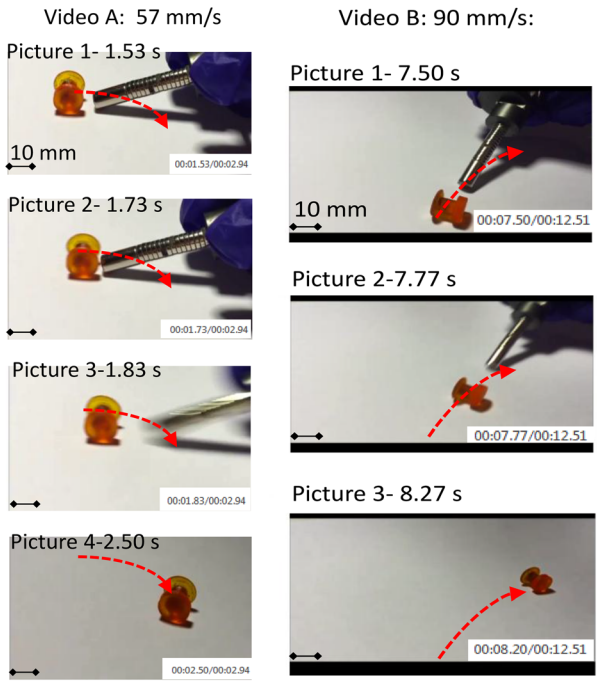

Fig. 9 Movements of the roller under external magnetic fields

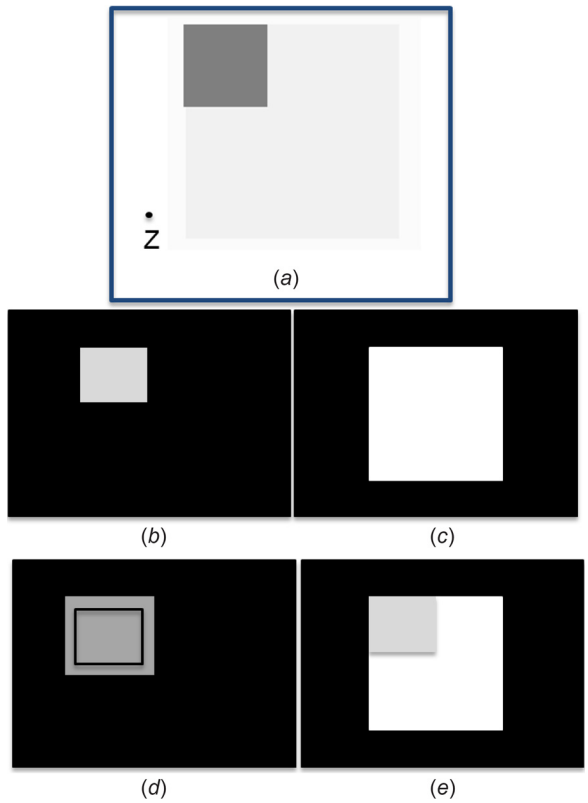

Fig. 10 Digital design and process planning for a square film test case: (*a*) digital design, (*b*) sliced deposition image, (*c*) sliced curing image, (*d*) particle dispersion before curing, and (*e*) curing pattern

and the designed path was calculated as the rolling motion error. Six experiment replications were conducted. It was found that with a rolling length of 44.5 mm, the rolling motion error was 1.14 ±0.9 mm.

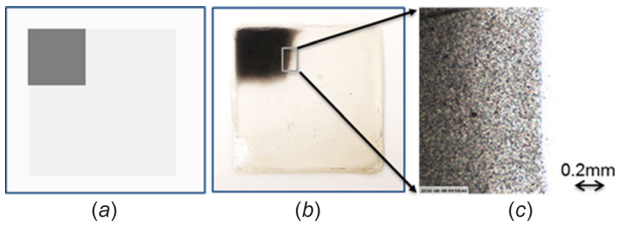

Fig. 11 Square film fabricated by the developed M-PSL process: (*a*) digital design, (*b*) printed part, and (*c*) microscopic image of the boundary region between the particle-filling region and particle-free region

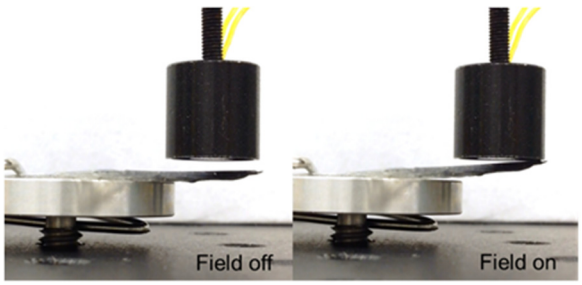

Fig. 12 Remote control the film by applying magnetic field

4.3 Test Case 3—Fabrication of a Smart Switch Using M-PSL

4.3.1 Model Design and Manufacturing Process. A deformable square film, which can work as a smart switch, was fabricated using the developed M-PSL process. A flexible resin FLGR01 from Formlabs and MRF-122EG from Mid-Atlantic Rubber are used as the feedstocks. The deformability is contributed by the flexible resin. In addition, embedded magnetic particles produce the desired responses to external magnetic fields. A digital design of the square film is shown in Fig. 10(*a*). In this test, to achieve the desired bending performance, magnetic particles are designed to deposit in a corner of the square film.

Given a volume loading fraction ∅ of 0.016, a 620 s exposure time was used for both the deposition image and curing image. A 0.65 mm thick film with heterogeneous properties was fabricated.

4.3.2 Fabricated Results. The fabricated square film is shown in Fig. 11. Microscopic images of the boundary region between embedded particles and pure resin are shown in Fig. 11(*c*).

An electromagnet is used as an external stimulus to trigger the bending movement of the square film. By turning the magnetic field on, the corner filled with magnetic particles will be attracted to the electromagnet, working as an off-switch. Experiments were also performed to characterize the on–off switch motion accuracy. It was found that by controlling the electrical input of the electromagnet, the flexible film can achieve a 100% on–off switch accuracy with a frequency up to 4 Hz.

5 Conclusions and Future Work

A novel mask image projection stereolithography process assisted by an external magnetic field was successfully developed for fabrication of magnetic-field responsive smart materials. Assisted by an external magnetic field, magnetic particles were selectively deposited in liquid resin and distributed with various patterns. Mask image was then projected to cure the photopolymer filled with magnetic particles.

The developed process is capable of achieving various magnetic particle-filling rate, filling pattern and structure, thus producing smart materials with complicated and heterogeneous

functions. As a concept-of-proof, three test cases have been performed. The experimental results demonstrate the feasibility and effectiveness of the proposed magnetic field-assisted projection stereolithography (M-PSL) technology in production of smart materials.

Future work will include: (1) Investigate methods for controlling the particle deposition more accurately; (2) Characterize the relationship between magnetic particle filling parameters, including filling rate, patterns, and orientations, on the macroscopic performance of the fabricated composite; and (3) Investigate the use of this technology in producing more complicated designs and smart machines.

References

[1] Filipcsei, G., Ildikó, C., András, S., and Miklós, Z., 2007, "Magnetic Field-Responsive Smart Polymer Composites," *Oligomers-Polymer Composites-Molecular Imprinting*, Springer, Berlin, pp. 137–189.

[2] Pacchioni, G., 2013, "Smart Materials From Nanotechnology for Global Challenges," J. Nanotechnol. Smart Mater., **1**, p. 1.

[3] Armentano, I., Dottori, M., Fortunati, E., Mattioli, S., and Kenny, J. M., 2010, "Biodegradable Polymer Matrix Nanocomposites for Tissue Engineering: A Review," Polym. Degrad. Stab., **95**(11), pp. 2126–2146.

[4] Gandhi, M. V., and Thompson, B. D., 1992, *Smart Materials and Structures*, Springer Science & Business Media/Chapman & Hall, New York/London.

[5] Hoffman, A. S., 2013, "Stimuli-Responsive Polymers: Biomedical Applications and Challenges for Clinical Translation," Adv. Drug Delivery Rev., **65**(1), pp. 10–16.

[6] Hu, J., Meng, H., Li, G., and Ibekwe, S. I., 2012, "A Review of Stimuli-Responsive Polymers for Smart Textile Applications," Smart Mater. Struct., **21**(5), p. 053001.

[7] Hussain, F., Hojjati, M., Okamoto, M., and Gorga, R. E., 2006, "Review Article: Polymer-Matrix Nanocomposites, Processing, Manufacturing, and Application: An Overview," J. Compos. Mater., **40**(17), pp. 1511–1575.

[8] Ionov, L., 2013, "3D Microfabrication Using Stimuli-Responsive Self-Folding Polymer Films," Polym. Rev., **53**(1), pp. 92–107.

[9] Meng, H., and Li, G., 2013, "A Review of Stimuli-Responsive Shape Memory Polymer Composites," Polymer, **54**(9), pp. 2199–2221.

[10] Okano, T., ed., 1998, *Biorelated Polymers and Gels: Controlled Release and Applications in Biomedical Engineering*, Academic Press, Cambridge, MA.

[11] Reece, L., 2007, *Smart Materials and Structures: New Research*, Nova Publishers, New York.

[12] Kim, K. J., and Shahinpoor, M., 2003, "Ionic Polymer–Metal Composites—II: Manufacturing Techniques," Smart Mater. Struct., **12**(1), p. 65.

[13] Huang, S. H., Liu, P., Mokasdar, A., and Hou, L., 2013, "Additive Manufacturing and Its Societal Impact: A Literature Review," Int. J. Adv. Manuf. Technol., **67**(5–8), pp. 1191–1203.

[14] Khalil, S., Nam, J., and Sun, W., 2005, "Multi-Nozzle Deposition for Construction of 3D Biopolymer Tissue Scaffolds," Rapid Prototyping J., **11**(1), pp. 9–17.

[15] Zhou, C., Chen, Y., Yang, Z. G., and Khoshnevis, B., 2011, "Development of Multi-Material Mask-Image-Projection-Based Stereolithography for the Fabrication of Digital Materials," Solid Freeform Fabrication Symposium (SFF), Austin, TX, Aug. 8–10, pp. 65–80.

[16] Jackson, B., Wood, K., and Beaman, J., 2000, "Discrete Multi-Material Selective Laser Sintering (M 2 SLS): Development for an Application in Complex Sand Casting Core Arrays," Solid Freeform Fabrication, Austin, TX, pp. 176–182.

[17] Liew, C. L., Leong, K. F., Chua, C. K., and Du, Z., 2001, "Dual Material Rapid Prototyping Techniques for the Development of Biomedical Devices—Part 1: Space Creation," Int. J. Adv. Manuf. Technol., **18**(10), pp. 717–723.

[18] Liew, C. L., Leong, K. F., Chua, C. K., and Du, Z., 2002, "Dual Material Rapid Prototyping Techniques for the Development of Biomedical Devices—Part 2: Secondary Powder Deposition," Int. J. Adv. Manuf. Technol., **19**(9), pp. 679–687.

[19] Santosa, J., Jing, D., and Das, S., 2002, "Experimental and Numerical Study on the Flow of Fine Powders From Small-Scale Hoppers Applied to SLS Multi-Material Deposition—Part I," Solid Freeform Fabrication Symposium (SFF), Austin, TX, Aug. 5–7, pp. 620–627.

[20] Bartolo, P. J., and Gaspar, J., 2008, "Metal Filled Resin for Stereolithography Metal Part," CIRP Ann.-Manuf. Technol., **57**(1), pp. 235–238.

[21] Kumar, S., and Kruth, J. P., 2010, "Composites by Rapid Prototyping Technology," Mater. Des., **31**(2), pp. 850–856.

[22] Wurm, G., Tomancok, B., Holl, K., and Trenkler, J., 2004, "Prospective Study on Cranioplasty With Individual Carbon Fiber Reinforced Polymere (CFRP) Implants Produced by Means of Stereolithography," Surg. Neurol., **62**(6), pp. 510–521.

[23] Pan, Y., Zhou, C., Chen, Y., and Partanen, J., 2014, "Multitool and Multi-Axis Computer Numerically Controlled Accumulation for Fabricating Conformal Features on Curved Surfaces," ASME J. Manuf. Sci. Eng., **136**(3), p. 031007.

[24] Bártolo, P. J., ed., 2011, *Stereolithography: Materials, Processes and Applications*, Springer Science & Business Media, Berlin.

[25] Pan, Y., and Chen, Y., 2015, "Smooth Surface Fabrication Based on Controlled Meniscus and Cure Depth in Microstereolithography," J. Micro Nano-Manuf., **3**(3), p. 031001.

[26] Pan, Y., Zhao, X., Zhou, C., and Chen, Y., 2012, "Smooth Surface Fabrication in Mask Projection Based Stereolithography," J. Manuf. Process., **14**(4), pp. 460–470.

[27] Pan, Y., Zhou, C., and Chen, Y., 2012, "A Fast Mask Projection Stereolithography Process for Fabricating Digital Models in Minutes," ASME J. Manuf. Sci. Eng., **134**(5), p. 051011.

[28] Tumbleston, J. R., Shirvanyants, D., Ermoshkin, N., Janusziewicz, R., Johnson, A. R., Kelly, D., Chen, K., Pinschmidt, R., Rolland, J. P., Ermoshkin, A., and Samulski, E. T., 2015, "Continuous Liquid Interface Production of 3D Objects," Science, **347**(6228), pp. 1349–1352.

[29] Mid-Atlantic, Inc., 2015, "MRF-122EG Magneto-Rheological Fluid," Mid-Atlantic Rubber Co., Baltimore, MD, accessed Dec. 20, 2016, http://www.lordmrstore.com/lord-mr-products/mrf-122eg-magneto-rheological-fluid